**Geoscientific
Model Development
Discussions**

The Joint UK Land Environment Simulator (JULES), Model description – Part 1: Energy and water fluxes

M. J. Best[1]**, M. Pryor**[2]**, D. B. Clark**[3]**, G. G. Rooney**[1]**, R. L. H. Essery**[4]**,
C. B. Ménard**[4]**, J. M. Edwards**[1]**, M. A. Hendry**[1]**, A. Porson**[1]**, N. Gedney**[2]**,
L. M. Mercado**[3]**, S. Sitch**[5]**, E. Blyth**[3]**, O. Boucher**[1]**, P. M. Cox**[6]**,
C. S. B. Grimmond**[7]**, and R. J. Harding**[3]

[1]Met Office, FitzRoy Road, Exeter, EX1 3PB, UK
[2]Met Office, JCHMR, Wallingford, UK
[3]Centre for Ecology and Hydrology, Wallingford, UK
[4]University of Edinburgh, Edinburgh, UK
[5]University of Leeds, Leeds, UK
[6]University of Exeter, Exeter, UK
[7]King's College London, London, UK

Correspondence to: M. J. Best (martin.best@metoffice.gov.uk)

Abstract

This manuscript describes the energy and water components of a new community land surface model called the Joint UK Land Environment Simulator (JULES). This is developed from the Met Office Surface Exchange Scheme (MOSES). It can be used as a stand alone land surface model driven by observed forcing data, or coupled to an atmospheric global circulation model. The JULES model has been coupled to the Met Office Unified Model (UM) and as such provides an opportunity for the research community to contribute their research into world-leading operational weather forecasting and climate change prediction systems. JULES has a modular structure aligned to physical processes, providing the basis for a flexible modelling platform.

1 Introduction

Traditionally Land Surface Models (LSMs) have been considered as the lower boundary condition for Global Circulation Models (GCMs) and other atmospheric modelling systems. Over the last couple of decades, the importance of the influence that the land surface has on atmospheric modelling has increased, which has led to additional focus on the complexity and accuracy of LSMs. Models have developed from a simple energy balance with a simple soil scheme (e.g., Deardorff, 1978) through to complex vegetation structures with multiple layer soil hydrology.

The large differences in the response of the surface fluxes to various surfaces has initiated a representation of sub-gridscale heterogeneity, such as tile or mosaic schemes (e.g., Essery et al., 2003). Differences at the surface can be caused by their interaction with snow (e.g., snow on top of the surface as with bare soil and short vegetation, or snow under the "surface" as with needleleaf forests), the availability of water at the surface, influencing the Bowen ratio (e.g., open water, snow and ice surfaces compared to vegetation and bare soil surfaces), or in the treatment of the

carbon cycle for vegetation (e.g., the difference in carbon pathways between C_3 and C_4 vegetation). Further increases in model resolution, particularly for regional scale operational weather forecasting, open up new challenges in the way we represent the sub-gridscale heterogeneity at the surface, as the nature of the heterogeneity changes.

5   As the resolution and accuracy of atmospheric modelling systems increases, there is likely to be a need for a wider diversity of land surface processes, such as river flow and flooding, groundwater, or potential crop yields. These new processes present some challenges as model developers will have to acquire new areas of expertise and integrate new science in existing modelling systems.

10   The development in our understanding of the interactions between the atmosphere and the biosphere for the carbon cycle has begun a new era for science in land surface modelling (e.g., Cox et al., 2000). Current research activities are not limited to the carbon cycle, but are also considering other elements such as the nitrogen cycle, methane and ozone (Thornton et al., 2007, 2009; Sokolov et al., 2008; Fisher et al., 2010; Zaehle et al., 2010). Again, the complexity of these new systems require additional expert

15 knowledge that has traditionally not been held by the original LSM developers.

It is beyond most research and operational centres to have the expertise in such a diverse range of science. Therefore to develop a state of the art LSM requires an alternative perspective to the traditional isolated development of these modelling sys-

20 tems. The development of a community land surface model enables experts in areas of land surface science to contribute towards a leading land surface model, from which all users will benefit. This is the concept adopted with the new community land surface model, the Joint UK Land Environment System (JULES). JULES originated from the Met Office Surface Exchange Scheme (MOSES; Cox et al., 1999; Essery et al.,

25 2003), the land surface model developed at the UK Met Office for applications ranging from operational weather forecasting to Earth system modelling. The forcing data required by JULES (Table 1) are the standard information that would be exchanged when coupled to an atmospheric GCM. Hence, JULES can be linked to the UK Met Office Unified Model (Cullen, 1993) opening up the opportunity for the research community to

JULES energy and water

M. J. Best et al.

Printer-friendly Version

Interactive Discussion

contribute its science into leading operational weather forecasting and climate change prediction systems.

In addition to the initialisation of the prognostic variables within the JULES model, ancillary information is required for various soil parameters (Table 2). These data are required for both stand alone and coupled applications.

JULES has been designed to be a flexible modelling system with a modular structure. This structure is illustrated in Fig. 1, where the connections between the modules show the physical processes that connect these areas. Within the modules there are also various science options (Table 3), which can be selected through a series of switches. The aim of this modular structure is to make it easy to replace modules or to introduce new modules within the modelling system. In addition to the main science modules within JULES there are also three themes. These themes are not connected by physical processes to the other modules, but do impact on each of them and are critical to ensure that the JULES modelling system remains a flexible, easy to use and develop, openly validated tool that can have identifyable configurations for applied applications. These themes include the technical design of the modelling system, the validation and callibration of all aspects of the model, and setting configurations of the modelling system that are suitable for climate impact studies. The themes surround the science modules in Fig. 1 demonstrating their integrating nature.

This paper, the first of two parts that describe the JULES system, is concerned with the energy and water cycles. The second part describes the additional modules required to represent the carbon cycle (Clark et al., 2011), whilst a companion paper addresses one of the cross cutting themes with benchmarking (Blyth et al., 2010). The sections of this paper describe the modules in Fig. 1 relating to energy and water. Section 2 describes the surface exchange, covering (Sect. 2.1) the energy balance equations, (Sect. 2.2) the surface resistance of moisture for vegetation, (Sect. 2.3) evaporation of moisture on the surface in either liquid or solid states, (Sect. 2.4) how urban areas are represented, and (Sect. 2.5) the treatment of surface heterogeneity.

Section 3 decribes the processes relating to snow. This includes (Sect. 3.1) the interaction of snow with vegetation canopies, two methods for modelling the snow on the ground, with either (Sect. 3.2) zero layer or (Sect. 3.3) multi-layer models, and (Sect. 3.4) the representation of snow albedo.

Section 4 deals with soil processes for temperature and moisture. This includes (Sect. 4.1) the amount of water that reaches the soil surface through vegetation canopies and how this is then distributed into runoff and infiltration, (Sect. 4.2) how soil moisture is extrated from the soil profile by vegetation, (Sect. 4.3) the thermodynamics and water transport within the soil, (Sect. 4.4) the hydraulic and (Sect. 4.5) thermal characteristics of the soil, (Sect. 4.6) the treatment for preventing a soil layer from becoming super-saturated, and finally (Sect. 4.7) the representation of heterogeneity for soil moisture. This is done via two posible methods, the first (Sect. 4.7.1) being based upon the TOPMODEL approach (Beven and Kirkby, 1979), and the second (Sect. 4.7.2) the PDM model (Moore, 1985).

2 Surface fluxes and energy balance

The surface fluxes of heat, moisture and momentum are calculated in JULES within the surface exchange module. To give the maximum flexibility in terms of the representation of surface heterogeneity and for the coupling of the land surface scheme to an atmospheric model, two generic types of surface are considered; vegetated and non-vegetated. The main difference between these two types of surface is the way in which the surface related parameters (e.g., albedo, roughness length) are specified. For non-vegetative surfaces they are specified by the user (with the exception of the MORUSES option for an urban surface, see Sect. 2.4), whereas for vegetated surfaces these parameters are derived from the structure of the vegetation itself. This leads to an alternative set of parameters that needs to be specified (e.g., rate of change of surface albedo with leaf area index, rate of change of roughness length with canopy height).

2.1 Surface exchange equations

The standard surface energy balance equations, used to calculate the distribution of availble energy between the various fluxes at the surface, have been extended to provide more flexibility to include additional physical processes. Thermal inertia is associated with the surface mass which is coupled to the underlying soil by three physical mechanisms depending upon the type of surface. The vegetation fraction is coupled to the soil using radiative exchange and atmospheric turbulence, whereas the remainder are coupled through conduction. The surface energy balance equation is then written:

$$C\frac{\delta T_*}{\delta t} = (1-\alpha)Sw_{\downarrow} + \epsilon L w_{\downarrow} - \sigma\epsilon(T_*)^4 - H - L_c E - G \tag{1}$$

where:

$$H = \frac{\rho c_p}{r_a}(T_* - T_1) \tag{2}$$

$$E = \frac{\rho}{r_a + r_s}(Q_{sat}(T_*) - Q_1) \tag{3}$$

$$G = v\left[\sigma\epsilon\,\epsilon_s(T_*)^4 - \sigma\epsilon\,\epsilon_s(T_{s1})^4 + \frac{\rho c_p}{r_{a_{can}}}(T_* - T_{s1})\right] + (1-v)A_s(T_* - T_{s1}) \tag{4}$$

Table 4 gives the definitions of the symbols.

A number of options can be chosen to adjust the formulation of the surface energy balance equations. The traditional surface energy balance equations can be obtained by setting the surface heat capacity to zero (i.e., setting the left-hand side of Eq. (1) to zero) and having only conductive coupling between the surface and the underlying soil (i.e., by setting the vegetation fraction variable to zero in Eq. 4). A second option enables the radiative and turbulent coupling between the soil and the surface canopy for vegetation, but still retains a zero surface heat capacity ($C = 0$), whilst the third option utilises the full energy balance equations above (Eqs. 1–4). Forthly, in addition

to utilising the full energy balance equations, there is an option which adjusts how snow is represented on vegetation by enabling the snow to exist below the canopy (see Sect. 2.3).

In order to obtain a fully implicit solution, each of the prognostic terms in the surface flux equations (apart from the soil temperature) are written in the form $X^{i+1} = X^i + \Delta X$. The equations are then linearised by assuming that $\Delta X \ll X$. This gives a new set of surface flux equations that can be written in the form of a fully explicit flux, an update to give an implicit solution and a further update to ensure that the atmospheric temperature and humidity satisfy implicit coupling with the atmosphere. The last update is only applied if JULES is connected to an atmospheric model with implicit coupling. So, for example, the surface moisture flux equation becomes:

$$E = \frac{\rho}{r_a + r_s} \left(Q_{sat}\left(T_*^i\right) - Q_1^i \right) + \frac{\rho}{r_a + r_s} \alpha \, \Delta T_* - \frac{\rho}{r_a + r_s} \Delta Q_1 \tag{5}$$

where $\alpha = \frac{\delta Q_{sat}}{\delta T}$ is evaluated at T_*^i. The implicit update to the fluxes comes from solving the surface flux equations, whilst the implicit coupling to the atmosphere comes from the coupling methodology of Best et al. (2004).

The aerodynamic resistance is calculated using standard Monin–Obukhov similarity theory (Monin and Obukhov, 1954), using the stability functions of Dyer (1974) for unstable conditions and Beljaars and Holtslag (1991) for stable conditions. The surface resistance for surfaces with potential evaporation (i.e., lake, snow and ice surfaces) is set to zero, whilst for an urban surface the conductance is set to zero unless water is available on the urban surface (i.e., the urban "canopy water"). For a bare soil surface, the surface conductance (g_{soil}, inverse of resistance) is determined by the soil moisture concentration in the top soil layer (θ_1):

$$g_{soil} = \frac{1}{100} \left(\frac{\theta_1}{\theta_c} \right)^2 \tag{6}$$

where θ_c is the soil moisture concentration at the critical point.

For vegetation, the surface resistance is calculated using the photosynthesis model described in Sect. 2.2.

For the vegetative surfaces, the latent heat flux is determined from a combination of evapotranspiration and bare soil evaporation. The relative fractions for each of these is determined by the density of the leaves, through the leaf area index. The combined flux represents the interaction of the atmosphere with both the canopy and the soil beneath.

2.2 Photosynthesis and stomatal conductance

The leaf level stomatal conductance (g_s) and net photosynthetic uptake (A) are linked via the CO_2 diffusion equation:

$$A = \frac{g_s}{1.6(C_c - C_i)} \qquad (7)$$

where C_c and C_i are the leaf surface and internal carbon dioxide concentrations, respectively.

A second equation by Jacobs (1994), which shares similarities with the simplified form of the Leuning (1995) stomatal conductance formulation, relates the ratio of internal to external CO_2 concentrations to leaf humidity deficit, D,

$$\frac{C_i - C_*}{C_c - C_*} = f_o\left(1 - \frac{D}{D_*}\right) \qquad (8)$$

where C_* is the CO_2 compensation point (Pa) and f_o and D_* are vegetation specific calibration parameters, which are directly related to the parameters from the Leuning (1995) model (for details, see Cox et al., 1998). This simplified formulation is convenient for large scale model applications (Cox et al., 1998). Potential (non-water stressed) leaf level photosynthesis (A_P) is calculated in JULES using the C_3 and C_4 photosynthesis models of Collatz et al. (1991) and Collatz et al. (1992), respectively. Photosynthesis is simulated as the minimum of three limiting rates: i) Rubisco limited

rate (W_C), ii) light limited rate (W_L) and iii) rate of transport of photosynthetic products (in the case of C_3 plants) and PEPCarboxylase limitation (in the case of C_4 plants) W_E. With both, W_C and W_L having a dependency on the leaf internal CO_2 concentration, C_i.

$$A_P = \min(W_C, W_L, W_E) \tag{9}$$

Leaf photosynthesis A, is related to the potential (non-stressed) leaf photosynthesis (A_P) as follows,

$$A = A_P \beta \tag{10}$$

β is the dimensionless moisture stress factor, which is related to the mean soil moisture concentration in the root zone, θ, and the critical and wilting point concentrations, θ_C and θ_W, respectively, as follows:

$$\beta = \begin{cases} 1 & \text{for } \theta \geq \theta_c \\ \frac{\theta - \theta_w}{\theta_c - \theta_w} & \text{for } \theta_w < \theta < \theta_c \\ 0 & \text{for } \theta \leq \theta_w \end{cases} \tag{11}$$

JULES uses either a big leaf or a multi-layer approach to scale photosynthesis and conductance to the canopy level. In the big leaf approach, canopy level photosynthesis and conductance are calculated using leaf level fluxes and total canopy leaf area index (Cox et al., 1998) using Beer's law (Monsi and Saeki, 1953). Using the multilayer approach, radiation absorbed and photosynthesis are estimated using a user defined number of leaf area increments (canopy layers) within the canopy, with the total canopy level flux calculated as the sum of the fluxes from each individual canopy layer (Jogireddy et al., 2006; Mercado et al., 2007). Equations describing the biochemistry of leaf level photosynthesis (W_C, W_L and W_E) and scaling up methods from leaf to canopy level are outlined in Part 2, which describes the carbon cycle in JULES (Clark et al., 2011).

2.3 Freely evaporating surfaces

Evaporation from the surfaces represented within JULES comes from a number of sources. These include evapotranspiration (i.e., water extracted from the soil through vegetation) and bare soil evaporation, both of which include a surface resistance that represents the restrictions in availability of water at the surface. The other sources of evaporation come directly from moisture stores and hence have no surface resistance. These sources include evaporation from open water surfaces, evaporation from surface water held in the canopy of vegetation or ponding on urban surfaces, and sublimation from snow.

The evaporation from water held on the leaves within the vegetation canopy will deplete the canopy water store and can result in all of the water being removed within a timestep. If this occurs, then the moisture unlimited evaporation is set to the amount of canopy water remaining, and any additional evaporation then comes through evapotranspiration with an associated stomatal, or surface, resistance. Such a limitation in the evaporative flux changes the surface energy balance equations, so an adjustment is made to each of the terms in the energy balance equations to ensure that the model has a consistent solution.

Each surface type within JULES can have snow on it. When snow is present, the surface resistance is set to zero to represent the fact that there is a moisture source. Within JULES there is also an option to have the snow lying underneath vegetation for the turbulent moisture flux (Sect. 3.1). In this case, an additional aerodynamic resistance is added to represent the efficiency of the turbulence at transporting moisture through the canopy. Any sublimation that occurs from the snow on the surface is used to deplete the snow mass in an analogous way to the canopy water. Also like the canopy water, if the snow is removed within a timestep, then an adjustment is made to the terms in the surface energy balance equations to ensure consistency.

Within JULES, lakes can be represented in two ways through the choice of available parameters. The default setting represents lakes as a bare soil surface, except that

the surface resistance for the turbulent moisture flux is set to zero, giving a freely evaporating surface. The second method makes use of the surface canopy in the energy balance equations by setting a suitably large value for the surface heat capacity (typically equivalent to water of a depth of around 1 m, although this can be altered by the user). This option reduces the diurnal cycle of the lake surface temperature compared to the first option, giving a more realistic simulation.

For both methods, as the lake is not explicitly modelled, the evaporative flux is not removed from any moisture store within the model, since it is assumed that there is sufficient water within the lakes to ensure that they are maintained. Similarly, any precipitation that falls onto the lake surface does not contribute to any water store. This means that in order to maintain a water balance, the integrated evaporative flux from the lake surface must be determined and included in the balance equations. This is not routinely done within JULES and has to be calculated through the available diagnostics by the user.

Similarly, the permanent ice surface does not have a prognostic water store, and hence care is required to maintain water balance. To represent an ice surface in JULES, the soil temperature profile is adopted to represent the thermal structure of the ice, whilst the moisture transport used in the soil scheme is neglected. This means that it is not possible to have a fractional coverage of land ice within a gridbox or source area. As such, there has to be either 100% of land ice cover or none.

As with snow cover (Sect. 3), the surface temperature of the ice surface is prevented from rising above the melting point of water, with any resulting residual of the surface energy balance being added to the melt flux. This means that care must be taken when setting land ice within the JULES model, especially when coupled to an atmospheric model. Small areas of ice could result in large thermal gradients in the atmosphere, caused by this restriction on the surface temperature compared to ice-free land. This can result in unrealistic small scale circulations and ultimately numerical problems. Hence this surface type should only be used to represent a large extent of permanent land ice.

⏮   ⏭

◀   ▶

Back   Close

Full Screen / Esc

Printer-friendly Version

Interactive Discussion

2.4   Representation of urban areas

The nature and design of urban environments make their surface energy balance significantly different from natural surfaces. However, a simple bulk representation for an urban area can be obtained by introducing a suitably large thermal capacity for the surface, along with radiative coupling between the surface and the underlying soil. Best (2005) showed that such a simple representation can lead to significant improvements within numerical weather prediction models. The advantage of this approach is that it can fit within JULES by adapting currently available parameters.

A second option to represent urban areas in JULES, is to use an additional surface tile. Best et al. (2006) showed that representing the roofs of buildings as one surface and street canyons as a second effective surface gives improvements over the one-tile approach. Also, Harman and Belcher (2006) and Porson et al. (2009) demonstrated that these two surfaces give a good approximation of more complex schemes that represent each of the facets within the urban area. The differences between the two surface types is given through the surface parameter specifications.

The third option implemented is the Met Office Reading Urban Surface Exchange Scheme (MORUSES), as described in Porson et al. (2010a,b). Again a two-tile scheme, but as the surface parameters are determined from the morphology and material properties of the city, this enables a distribution of surface fluxes with different structural properties. The radiative exchange within the canyon tile is formulated with an effective albedo and an effective emissivity, based upon the exchanges between the various street canyon facets. The roughness length for momentum for the urban area is determined from the formulation of Macdonald et al. (1998), for a staggered array of cubes; the canyon and the roof tiles both have the same roughness.

The roughness length for temperature comes from a physically-based parametrization that relates to the urban morphology and uses a resistance network to represent the transfer of heat. The canyon tile includes the effects of the recirculation jets by using two resistance pathways; one for each of the recirculation and ventilation regions. For

both of these elements, three resistances are used, two representing the heat across an internal boundary layer adjacent to each facet and one representing the transfer of heat across the inertial sub-layer. The roof, which is simpler, only has two resistances representing the internal boundary layer and inertial sub-layer (see Harman et al., 2004; Porson et al., 2010a, for more details).

Effective areal heat capacities are determined to represent the roof and the canyon, which includes contributions from both the walls and the road. These are determined by considering the diurnal response using a force-restore model, whilst an adjustable roof parameter is also introduced to increase the flexibility to capture different oscillations. The canyon tile is conductively coupled through the road to the underlying soil surface, whilst the walls of the canyon and the roof tile are decoupled from the soil, by imposing a zero flux boundary condition.

2.5 Surface heterogeneity

The heterogeneity of the surface is modelled within JULES by using the tile, or mosaic, approach (e.g., Essery et al., 2003). This means that a separate surface energy balance is determined for each type of surface within the domain of the gridbox or footprint, and the individual surface fluxes are then given a weighted average in order to determine the gridbox or footprint mean flux into the atmosphere. One limitation to the current structure of JULES is that although the surface exchange represents the heterogeneity through tiling, there is no representation of sub-gridscale heterogeneity within the sub-surface soil module beyond the choise of parameters that are used. This will be developed in future versions of the JULES model.

In order to keep the parametrization of surface heterogeneity as flexible as possible, the number of surface types to be considered within a model simulation is determined at run time. Hence the complexity of the heterogeneity and cost in terms of computational time have to be balanced. Thus a time-limited modelling application, such as operational weather forecasting, can run with minimal surface types to optimize cost, whereas other applications may benefit from unlimited surface types (e.g., climate applications with an interactive carbon cycle).

Full Screen / Esc

Printer-friendly Version

Interactive Discussion

There are two generic types of surface in JULES having differing requirements for their surface parameters: (1) Non-vegetated surfaces have fixed values (e.g., albedo and roughness length) which are specified at run time, and (2) vegetated surfaces whose parameters vary. The latter are calculated in the following paragraphs.

5   The roughness length for momentum (z_0) for vegetation is determined from

$$z_0 = \omega h \tag{12}$$

where h is the canopy height and ω accounts for the rate of change of roughness length with the canopy height by vegetation type.

There are two options to determine the surface albedo (α) for vegetation. The sim-
10 plest option is a bulk albedo:

$$\alpha = \alpha_0 \exp(-kL) + \alpha_\infty[1 - \exp(-kL)] \tag{13}$$

where α_0 is the soil albedo, which is a spatially varying ancillary field within JULES, α_∞ is the prescribed maximum canopy albedo for dense leaf coverage, L is the leaf area index and k is a light extinction coefficient.
15 With the second option, the snow-free albedos are calculated using the two-stream model for radiative transfer through vegetation described by Sellers (1985). This scheme uses separate direct-beam and diffuse albedos in the visible and near-infrared wave bands for each vegetation type. This requires four parameter values for leaf reflection coefficients and leaf scattering coefficients for both near infra-red and photo-
20 synthetically active radiation.

An additional parameter for vegetation surfaces is the capacity of the canopy to hold water (c_m) through the interception of precipitation,

$$c_m = A + BL \tag{14}$$

where B is the rate of change of capacity with leaf area index which varies between
25 vegetation type, and A is the puddling of water on the soil surface and interception by leafless plants by vegetation type.

By default nine surface types are represented; five vegetation (broadleaf trees, needleleaf trees, C_3 grasses, C_4 grasses and shrubs) and four non-vegetated surfaces (urban, open water, bare soil and permanent land ice). The default parameters for each of these surface types are given in Tables 5 and 6.

5   In addition to the surface type, each has an elevation above the mean gridbox height. This enables surfaces that are sensitive to the changes in atmospheric temperature and humidity, arising from displacement above the mean surface height, to experience adjusted atmospheric forcing. This is done in a simple way by adjusting the air temperature along a dry adiabat whilst keeping the humidity constant until the saturation

10   point is reached. After this, the temperature is adjusted along a moist adiabat, whilst the humidity is then set to the saturated humidity at the new atmospheric temperature. To ensure consistency with the top soil level temperature, this is adjusted by the same increment as the air temperature. This prevents artificial warming from the soil without having to introduce heterogeneity into the soil. This assumption will be removed

15   once soil heterogeneity is introduced into the JULES code. One impact of introducing elevation bands is to reduce artificial sublimation and melting from snow-covered surfaces.

3   Snow model

Two snow schemes are available within JULES. The simplest is a zero-layer snow

20   model that adapts the top soil level to include the snow processes. The more comprehensive and physically realistic scheme takes a multi-layer approach. Interaction of snow with a vegetation canopy is also possible.

3.1   Interaction of snow with vegetation canopies

Snow is held as a single store on each surface type or, for vegetation surfaces, may

25   be partitioned between snow on the canopy and the underlying ground (Essery et al.,

2003). The surface resistance for sublimation is set to zero for tiles with snow cover in the single-store option, but is

$$r_s = \frac{\rho_i r^2}{0.03 D(1.79 + 3U^{1/2})I}\left(\frac{I}{I_{max}}\right)^{0.4} \qquad (15)$$

for canopy snow, where I is the intercepted snow load, $I_{max} = 4.4L$ is the snow interception capacity for a canopy with leaf area index L, D is the diffusivity of water vapour in air, ρ_i is the density of ice and $r = 0.5$ mm is a nominal grain radius for intercepted snow. The change in load during a timestep with snowfall amount S_f on a canopy with initial load I_0 is

$$\Delta I = 0.7(I_{max} - I_0)\left(1 - e^{-S_f/I_{max}}\right). \qquad (16)$$

Unloading of snow from the canopy is set equal to 40% of the canopy snowmelt rate.

3.2 Zero-layer snow model

In the zero-layer snow model, snow is given a constant thermal conductivity and a constant density. The heat capacity of snow is neglected, but snow decreases the bulk thermal conductivity of the surface layer due to both the increased layer thickness and the different conductivities of snow and soil. For snow depth (d_s) less than half the surface soil layer thickness (Δz_1), the thermal conductivity (λ) used in surface energy balance calculations is adjusted for insulation by snow according to

$$\lambda = \lambda_{soil}\left[1 + \frac{2d_s}{\Delta z_1}\left(\frac{\lambda_{soil}}{\lambda_{snow}} - 1\right)\right]^{-1} \qquad (17)$$

The heat flux between the surface layer and the second soil layer, of thickness Δz_2, is multiplied by a snow insulation factor (ζ)

$$\zeta = \left(1 + \frac{2d_s}{\Delta z_1 + \Delta z_2}\right)^{-1}. \qquad (18)$$

For deeper snow, the surface conductivity is set equal to λ_{snow} and the insulation factor is

$$\zeta = (\Delta z_1 + \Delta z_2) \left[(2d_s - \Delta z_1) \frac{\lambda_{\text{soil}}}{\lambda_{\text{snow}}} + 2\,\Delta z_1 + \Delta z_2 \right]^{-1}. \tag{19}$$

The surface skin temperature is not allowed to exceed 0 °C while snow remains on the ground, and the heat flux used to melt snow is diagnosed as a residual in the surface energy balance. Melt water drains immediately from the snow and is partitioned into soil infiltration and runoff; there is no storage or freezing of liquid water in snow. The snow thermal conductivity, snow density and surface layer thickness are parameters that are set by the user.

3.3 Multi-layer snow model

The maximum number of layers (N_{max}) that are used for deep snow and their thickness d_k ($k = 1, \ldots, N_{\text{max}}$) are set by the user. However, the number of layers actually used depends on the snow depth, which means that not all the layers exist at any one time. When a layer is at the base of the snowpack it has a variable thickness. Shallow snow is combined with the surface soil layer for snow depth $d_s < d_1$ for numerical stability, whilst setting $N_{\text{max}} = 0$ forces the use of the zero-layer option for any depth of snow. For $d_s \geq d_1$, snow is represented by additional model layers on top of the soil if $N_{\text{max}} \geq 1$. As the snow depth increases, the lowest layer in the snowpack increases in thickness until it reaches twice its prescribed thickness; the layer then splits in two with the upper part staying fixed in thickness and the new lowest layer thickening as the snow accumulates. This is reversed as the snow depth decreases, with layers being progressively combined at the bottom of the snowpack. The division of a snowpack into layers is illustrated in Fig. 2. A variable snow density is used, so snow depth can decrease due to compaction as well as ablation.

Each layer in the snowpack has a thickness d_k (m), a temperature T_k (K), a density ρ_k (kg m^{-3}), an ice content I_k (kg m^{-2}) and a liquid water content W_k (kg m^{-2}). Layer

Back | Close

Full Screen / Esc

Printer-friendly Version

Interactive Discussion

thickness, density and mass are related by $\rho_k d_k = I_k + W_k$. The increase in layer density due to compaction over a timestep of length δt is calculated as

$$\frac{\delta \rho_k}{\delta t} = \frac{\rho_k \, g \, M_k}{\eta_0} \exp\left(\frac{k_s}{T_m} - \frac{k_s}{T_k} - \frac{\rho_k}{\rho_0}\right) \tag{20}$$

where g is the acceleration due to gravity, $k_s = 4000\,\text{K}$, compactive viscosity $\eta_0 = 10^7\,\text{Pa s}$, reference density $\rho_0 = 50\,\text{kg m}^{-3}$, temperature $T_m = 273.15\,\text{K}$, and $M_k = 0.5(I_k + W_k) + \sum_{i=1}^{k-1}(I_i + W_i)$ is the mass of snow above the middle of the layer. This scheme, based on measurements by Kojima (1967), has previously been used in the snow models described by Pitman et al. (1991) and Lynch-Stieglitz (1994). The areal heat capacity of a layer is

$$C_k = I_k \, C_{ice} + W_k \, C_{water} \tag{21}$$

where $C_{ice} = 2100\,\text{J K}^{-1}\,\text{kg}^{-1}$ and $C_{water} = 4180\,\text{J K}^{-1}\,\text{kg}^{-1}$ are the specific heat capacities of ice and water, and the thermal conductivity is

$$\lambda_k = 2.22 \left(\frac{\rho_k}{\rho_{water}}\right)^{1.88} \tag{22}$$

where $\rho_{water} = 1000\,\text{kg m}^{-3}$ is the density of water.

The structure of the multi-layer snow model is shown in Fig. 3. The conducted heat flux at the bottom of layer k is

$$H_k = \Gamma_k \left[T_k - T_{k+1} + \gamma \left(\delta T_k - \delta T_{k+1}\right)\right] \tag{23}$$

where δT_k is the increment in layer temperature over a timestep, γ is the forward timestep weighting (0 for explicit and 1 for fully implicit timestepping), and

$$\Gamma_k = \left(\frac{d_k}{2\lambda_k} + \frac{d_{k+1}}{2\lambda_{k+1}}\right)^{-1} \tag{24}$$

Full Screen / Esc

Printer-friendly Version

Interactive Discussion

For the lowest snow layer ($k = N$), T_{N+1}, d_{N+1} and λ_{N+1} are the temperature, thickness and conductivity of the surface soil layer. The increment in layer temperature over a timestep is

$$\delta T_k = \frac{\delta t}{C_k}(H_{k-1} - H_k) \tag{25}$$

5 Surface heat flux H_0 calculated by the surface exchange module is passed to the snow module, and ground heat flux H_N calculated by the snow module is passed to the soil module; implicit timestep weighting of surface soil layer temperature T_{soil} is not used in calculating this flux. For a single snow layer the temperature increment is given by

$$\delta T_1 = \frac{\delta t}{C_1}[H_0 - \Gamma_1(T_1 - T_{\text{soil}} + \gamma \, \delta T_1)] \tag{26}$$

10 with solution

$$\delta T_1 = \frac{[H_0 + \Gamma_1(T_{\text{soil}} - T_1)]\delta t}{\gamma \Gamma_1 \delta t + C_1} \tag{27}$$

When there are $N > 1$ snow layers, increments in the layer temperatures are found as the solutions of the tridiagonal set of equations

$$b_1 \, \delta T_1 + c_1 \, \delta T_2 = [H_0 + \Gamma_1(T_2 - T_1)]\delta t, \tag{28}$$

15 $$a_k \, \delta T_{k-1} + b_k \, \delta T_k + c_k \, \delta T_{k+1} = [\Gamma_{k-1}(T_{k-1} - T_k) + \Gamma_k(T_{k+1} - T_k)]\delta t \tag{29}$$

for $k = 2,\ldots,N-1$, and

$$a_N \, \delta T_{N-1} + b_N \, \delta T_N = [\Gamma_{N-1}(T_{N-1} - T_N) + \Gamma_N(T_1 - T_N)]\delta t \tag{30}$$

with matrix elements

$$a_k = c_{k-1} = -\gamma \Gamma_{k-1} \delta t \tag{31}$$

20 and

$$b_k = C_k + \gamma(\Gamma_{k-1} + \Gamma_k)\delta t. \tag{32}$$

If the temperature of a layer is calculated to be above T_m, the layer ice mass is reduced by an amount

$$\delta I_k = \frac{C_k}{L_f}(T_k - T_m) \tag{33}$$

or the entire mass of the layer, whichever is least; L_f is the latent heat of fusion. The layer liquid mass is increased by the same amount and the layer temperature is reset to T_m. Sublimation calculated by the surface exchange module is removed from the surface layer ice mass and from deeper layers if the surface layer sublimates entirely during a timestep.

A layer of depth d_k entirely consisting of liquid water would have a liquid content of $\rho_{water} \, d_k$. Snow layers are allowed to retain a fraction W_{cap} (set by the user) of this liquid content. When the liquid content of a layer exceeds its capacity, excess water is passed to the layer below. Liquid water in a layer with temperature below T_m will freeze, decreasing the liquid content by an amount

$$\delta W_k = \frac{C_k}{L_f}(T_m - T_k), \tag{34}$$

increasing the ice content by the same amount, and increasing the temperature by

$$\delta T_k = \frac{L_k \, \delta W_k}{C_k}. \tag{35}$$

The water flux at the base of the snowpack is passed to the surface hydrology module (Sect. 4.1).

Fresh snow is added as an interim layer 0 with density ρ_0 and temperature equal to the surface layer temperature. After increments have been applied to the layer masses and temperatures, layers are combined or split as necessary to match the fixed layer thicknesses, conserving liquid, solid and cold contents.

3.4 Snow albedo

Diagnostic and prognostic snow albedo options are provided. In the diagnostic scheme, a snow-free albedo α_0 and an albedo α_{cds} for cold deep snow are specified for each surface type. When the surface temperature exceeds a threshold temperature T_c, the snow albedo is decreased according to

$$\alpha_s = \alpha_{cds} + k(\alpha_0 - \alpha_{cds})(T_* - T_c). \tag{36}$$

For a tile with snow depth d_s, the albedo is a weighted average

$$\alpha = \alpha_0 + (\alpha_s - \alpha_0)(1 - e^{-d_s/d_m}) \tag{37}$$

for surface masking snow depth d_m.

For tall vegetation, the impact of snow lying underneath the vegetation canopy is taken into account by setting lower values for the cold deep snow albedo.

The prognostic albedo scheme uses the Wiscombe and Warren (1980) spectral snow model. The ageing of the snow surface is characterized by introducing a prognostic grain size $r(t)$, set to $r_0 = 50\,\mu m$ for fresh snow and limited to a maximum value of 2000 μm. The change in grain size over a timestep is given by

$$r(t + \delta t) = \left[r(t)^2 + \frac{G_r}{\pi} \delta t \right]^{1/2} - [r(t) - r_0] \frac{S_f \delta t}{d_0} \tag{38}$$

for snowfall rate S_f. The mass of fresh snow required to refresh the albedo (d_0), is set to 2.5 kg m^{-2}. The empirical grain area growth rate, in $\mu m^2\,s^{-1}$, is

$$G_r = \begin{cases} 0.6 & T_* = T_m \text{ (melting snow)} \\ 0.06 & T_* < T_m, \, r < 150\,\mu m \text{ (cold fresh snow)} \\ A\exp(-4550/T_*) & T_* < T_m, \, r > 150\,\mu m \text{ (cold aged snow)} \end{cases}$$

where $A = 0.23 \times 10^6\,\mu m^2\,s^{-1}$. Snow albedos for diffuse visible and near-infrared radiation are calculated as

$$\alpha_{vis} = 0.98 - 0.002(r^{1/2} - r_0^{1/2}) \tag{39}$$

and

$$\alpha_{nir} = 0.7 - 0.09 \ln\left(\frac{r}{r_0}\right). \tag{40}$$

The zenith-angle dependence of albedos for direct-beam radiation with zenith cosine μ is represented by using an effective grain size,

$$r_e = [1 + 0.77(\mu - 0.65)]^2 r, \tag{41}$$

in place of r in the equations for diffuse albedos (Eqs. 39 and 40).

For a tile with snow-free albedo α_0, snowdepth d_s and roughness length z_0, the albedo in each band is

$$\alpha = f_s \alpha_s + (1 - f_s)\alpha_0 \tag{42}$$

where

$$f_s = \frac{d_s}{d_s + 10 z_0}. \tag{43}$$

When driving data with separate direct-beam and diffuse radiation in visible and near-infrared bands are not available, the average of the diffuse albedos is simply used as an all-band snow albedo.

4   Hydrology and soil thermodynamics

JULES includes multi-layer, finite-difference models of sub-surface heat and water fluxes, as described in Cox et al. (1999). There are options for the specification of the hydraulic and thermal characteristics, the representation of super-saturated soil moisture and the sub-surface heterogeneity of soil moisture.

Printer-friendly Version

Interactive Discussion

4.1 Surface hydrology

To account for the size of convective storms compared to gridsize, a rainfall rate is assumed to fall on a fraction e_r of the grid. For largescale precipitation and point studies this fraction is set to one, whilst for convective precipitation it can take lower values, and is typically set to a value of 0.3.

The amount of water that reaches the soil surface depends upon the type of surface. For non-vegetation surfaces, this is simply the precipitation rate (R), whereas for vegetation surfaces, this becomes the throughfall (T_F) and is calculated using:

$$T_F = R\left(1 - \frac{C}{C_m}\right)\exp\left(-\frac{e_r C_m}{R\,\Delta t}\right) + R\frac{C}{C_m} \tag{44}$$

and the canopy water (C) is updated by

$$C^{(n+1)} = C^{(n)} + (R - T_F)\,\Delta t. \tag{45}$$

where C_m is the maximum canopy water that can be held by the vegetation and Δt is the timestep.

The canopy water can also be increased through dewfall (i.e., downward surface moisture fluxes), and is depleted by surface evaporation. Similarly, snow cover is increased through the deposition of frost (modelled as dewfall at surface temperatures below freezing), whilst the melting of snow contributes to the water available at the soil surface and updates the equivalent water within the snow pack.

The water reaching the soil surface is then split between infiltration into the soil and surface runoff. This is determined by the surface runoff (Y):

$$Y = \begin{cases} R\frac{C}{C_m}\exp\left(-\frac{e_r K C_m}{R C}\right) + R\left(1 - \frac{C}{C_m}\right)\exp\left(-\frac{e_r C_m}{R\,\Delta t}\right) & K\,\Delta t \le C \\ R\exp\left[-\frac{e_r (K\,\Delta t + C_m - C)}{R\,\Delta t}\right] & K\,\Delta t > C \end{cases}$$

where the surface infiltration rate K is equal to $\beta_s K_s$; K_s is the soil saturated hydrological conductivity and β_s is an enhancement factor.

Back | Close

Full Screen / Esc

Printer-friendly Version

Interactive Discussion

The infiltration into the soil (W_0) is determined through the integration of the contributions for each of the surface types by using the water balance at the surface:

$$W_0 = \sum_j v_j (T_{Fj} + S_{mj} - Y_j). \tag{46}$$

4.2 Soil moisture extraction

The ability of vegetation to access moisture at each level in the soil is determined by root density, assumed to follow an exponential distribution with depth. The fraction of roots in soil layer k extending from depth z_{k-1} to z_k is

$$r_k = \frac{e^{-2z_{k-1}/d_r} - e^{-2z_k/d_r}}{1 - e^{-2z_t/d_r}}, \tag{47}$$

where d_r is the rootdepth for the vegetation type and z_t is the total depth of the soil model. For transpiration E_t, the flux extracted from soil layer k is $e_k^0 E_t$, where

$$e_k^0 = \frac{r_k \beta_k}{\sum_k r_k \beta_k} \tag{48}$$

and

$$\beta_k = \begin{cases} 1 & \theta_k \geq \theta_c \\ (\theta_k - \theta_w)/(\theta_c - \theta_w) & \theta_w < \theta_k < \theta_c \\ 0 & \theta_k \leq \theta_w \end{cases}$$

is a soil moisture availability factor, defined similarly to Eq. (11), for a soil layer with unfrozen volumetric soil moisture concentration θ_k, critical point θ_c and wilting point θ_w.

4.3 Soil thermodynamics and water fluxes

The sub-surface at a gridpoint is either soil or land ice (with no water movement in the latter). Sub-surface temperatures are calculated using a finite difference form of

Title Page

Abstract | Introduction

Conclusions | References

Tables | Figures

◄ | ►◄

◄ | ►

Back | Close

Full Screen / Esc

Printer-friendly Version

Interactive Discussion

the heat diffusion equation, including the effects of solid-liquid phase changes of water. The temperature of the kth soil layer is incremented by the diffusive heat fluxes into and out of the layer, G_{k-1} and G_k, and the advective flux from the layer by flowing water, J_k:

$$C_a \Delta z_k \frac{dT_k}{dt} = G_{k-1} - G_k - J_k \Delta z_k \qquad (49)$$

5   where the fluxes are calculated as

$$G = \lambda \frac{\partial T}{\partial z}$$

$$J = c_w W \frac{\partial T}{\partial z}$$

where z is the vertical coordinate, W is the vertical flux of soil water and c_w is the specific heat capacity of water. C_a is the "apparent" volumetric heat capacity of the
10   layer, including the effect of phase changes (Cox et al., 1999). For soil, the sub-surface thermal characteristics are a function of solid and liquid water contents, while land ice uses fixed characteristics. The top boundary condition for Eq. (49) is the surface heat flux, calculated by the surface exchange module, while at the bottom there is a zero flux boundary condition to ensure conservation of energy.

15   The number of soil layers is a model parameter but the default is four of thicknesses 0.1, 0.25, 0.65 and 2.0 m, giving a total soil depth of 3 m. This configuration is designed to capture the variation of soil temperature from sub-daily to annual timescales (Best et al., 2005).

Soil water contents are updated using a finite difference form of the Richards equa-
20   tion. The moisture content of each layer (θ) is updated as:

$$\frac{d\theta_k}{dt} = W_{k-1} - W_k - E_k - R_{bk} \qquad (50)$$

where W_{k-1} and W_k are the diffusive fluxes flowing in from the layer above and out to the layer below, respectively, E_k is the evapotranspiration extracted by plant roots in

Back | Close

Full Screen / Esc

Printer-friendly Version

Interactive Discussion

the layer (and bare soil evaporation for the top layer) and R_{bk} is lateral runoff, which is set to zero unless the sub-surface heterogeneity of soil moisture is represented using the TOPMODEL option (Sect. 4.7.1). The fluxes follow Darcy's law

$$W = K \left(\frac{\partial \Psi}{\partial z} + 1 \right)$$

5   in which K is the hydraulic conductivity and Ψ is the soil water suction. The top boundary condition for Eq. (50) is the infiltration of water at the soil surface, whilst the lower boundary condition is drainage, which contributes to sub-surface runoff.

4.4 Hydraulic characteristics

There are two options for the hydraulic characteristics. In the first the relation between
10   soil water content, suction and hydraulic conductivity are Brooks and Corey (1964):

$$\theta/\theta_s = (\Psi/\Psi_s)^{-1/b} \qquad (51)$$
$$K = K_s(\theta/\theta_s)^{2b+3} \qquad (52)$$

where K_s is the hydraulic conductivity for saturated soil. The parameters θ_s, Ψ_s and b are calculated from soil texture information using the relationships of Cosby et al.
15   (1984) or others. (Note that Cox et al., 1999; incorrectly referenced Eqs. (51) and (52) as Clapp and Hornberger, 1978; rather than Brooks and Corey, 1964; Toby Marthews, personal communication, 2009.)

The second option uses the hydraulic relationships of van Genuchten (1980):

$$\frac{\theta - \theta_r}{\theta_s - \theta_r} = \frac{1}{[1+(\alpha\Psi)^n]^m} \qquad (53)$$

20   $$K = K_s S^{\xi} \left[1 - (1 - S^{1/m})^m \right]^2 \qquad (54)$$

where $m = 1 - 1/n$, $S = (\theta - \theta_r)/(\theta_s - \theta_r)$ and θ_r is the residual soil moisture concentration. In JULES, $\xi = 0.5$ and the soil moisture variable is implicitly defined as $\theta - \theta_r$,

Full Screen / Esc

Printer-friendly Version

Interactive Discussion

leaving three parameters. Dharssi et al. (2009) show that with suitable parameter values, Eqs. (51) and (53) are similar over most of the soil moisture range.

The soil parameter values can vary between layers but, in the absence of suitable data with which to specify this variation, many applications ignore any variation with depth. When calculating the hydraulic characteristics using Eqs. (51)–(54), JULES uses θ_u, the unfrozen volumetric water content, instead of θ, to capture the effects of soil freezing, following Cox et al. (1999).

4.5 Thermal characteristics

JULES has two options for calculating the effective thermal conductivity of soil λ. The first option is described by Cox et al. (1999):

$$\lambda = (\lambda_s - \lambda_{dry})\,\theta/\theta_s + \lambda_{dry}$$

where λ_s and λ_{dry} are the thermal conductivity for saturated and dry soil respectively and

$$\lambda_s = \lambda_{water}^{\theta_u^s}\,\lambda_{ice}^{\theta_f^s}\,\lambda_{dry}/\lambda_{air}^{\theta_s}$$

where λ_{air}, λ_{water} and λ_{ice} are the thermal conductivities of air, liquid water and frozen water, respectively, $\theta_f^s = \theta_s[S_f/(S_u + S_f)]$ and $\theta_u^s = \theta_s - \theta_f^s$. S_u and S_f are the unfrozen and frozen water contents as a fraction of saturation.

The second option uses the Dharssi et al. (2009) simplification of Johansen (1975):

$$\lambda = (\lambda_s - \lambda_{dry})K_e + \lambda_{dry}$$

where K_e is the Kersten number

$$K_e = \begin{cases} \log(\theta/\theta_s) + 1.0 & (\theta/\theta_s) \geq 0.1 \\ 0 & \text{otherwise} \end{cases}$$

$\lambda_s^u = 1.58 + 12.4(\lambda_{dry} - 0.25)$, with the constraint that $1.58 \le \lambda_s^u \le 2.2$, and

$$\lambda_s = \frac{\lambda_{liq}^{\theta_u^s} \lambda_{ice}^{\theta_f^s}}{\lambda_{liq}^{\theta_s}} \lambda_s^u$$

This generally gives larger values for conductivity than the Cox et al. (1999) formulation, which reduces the errors in simulated air temperature when used in numerical weather prediction (Dharssi et al., 2009).

4.6 Super-saturation of soil moisture

The numerical solution for the transport of soil moisture between the soil layers may result in layers which become super-saturated. JULES has two options to prevent this from occurring. With the first option, if a soil layer becomes super-saturated, then the soil moisture in this layer is limited to the saturation point and the excess water is prevented from moving into the layer from above, i.e. the drainage into the layer is restricted by the saturation. This results in the excess water being moved back up the soil layer, and if the top soil layer becomes super-saturated, then the excess water is added to the surface runoff.

The second option is to route the excess soil moisture to the soil layers below. This assumes excess soil moisture might flow laterally over land within a large grid-box, but would eventually move down through the soil layers at subgrid locations in which drainage is less impeded (e.g., where there is fractured permafrost or less compacted/faster draining soil types). This results in the excess water being moved down to lower layers, and if the bottom soil layer becomes super-saturated, then the excess water is added to the sub-surface runoff.

If the total soil column is saturated, then the difference between these two options is to add the excess water to either the surface or sub-surface runoff. Whilst in both cases the water results in a runoff flux, this could impact the timing of river flow due to the

delay of sub-surface runoff getting into the river network. Tests of the two options with the PILPS2d Valdai data (Schlosser et al., 2000) showed that moving the excess water in the downwards direction led to a poor surface runoff simulation and excessive soil moisture, whereas inhibiting the drainage of water into a saturated layer gave a better
5   agreement with observations.

However, global simulations have shown that in regions of partially frozen soils, one possible result is saturated and partially frozen soil layers near the surface, with unsaturated layers below. In this situation, the option to inhibit the drainage of water into the saturated layer at the surface leads to excessive surface runoff of snowmelt, giving
10   a dry soil during spring and hence a dry and warm bias in the atmosphere during the summer. The option to move the excess water to lower layers moistens the lower unsaturated soil layers and removes some of this dry and warm atmospheric bias whilst reducing the surface runoff of snowmelt.

These results suggest that the grid size may be important in determining the domi-
15   nant physical processes that prevent the super-saturation of the soil, and further work is required to determine how this should be represented in the model. Thus care should be taken when choosing between options for controlling super-saturation, with consideration being taken for the required application.

4.7   Soil moisture heterogeneity

20   There are two options in JULES to introduce heterogeneity into the soil moisture. One (TOPMODEL) represents this heterogeneity throughout the soil column, whereas the other (PDM) considers only heterogeneity in the top soil layer.

4.7.1   TOPMODEL

JULES can optionally use a parameterisation based on TOPMODEL (Beven and
25   Kirkby, 1979). TOPMODEL was initially designed to include a groundwater model within a single catchment where the height of the saturated zone moves up and down

Full Screen / Esc

Printer-friendly Version

Interactive Discussion

and is controlled by the recharge into it and the saturated lateral flow (baseflow) out. As the water table becomes higher, more of the surface area becomes saturated (and vice versa), with the regions of higher topographic index (λ_i) flooding first. Topographic index relates to the upstream area draining into a locality and the local slope, which is
5   a measure of the potential for flowout. Thus it is the potential to flood relative to other regions within the catchment.

This distributed catchment-based model is simplified into a semi-distributed model (Sivapalan et al., 1987) for use in climate models by lumping areas of similar topographic index together from one or potentially more catchments. A gridbox mean water
10 table depth $\bar{z}_w$ is calculated, and the probability distribution function (pdf) of the topographic index within the gridbox is then used to describe the relative frequency of occurrence of the topographic indices. The gridbox fraction of the water table that is above the surface may then be calculated. This enables saturation excess runoff to occur in the model before the gridbox soil moisture is totally saturated. Runoff occurs
15 when water is unable to permeate the fraction of the gridbox surface where the water table is above the surface.

The implementation of this approach in JULES was adapted by Gedney and Cox (2003) and Clark and Gedney (2008). With the TOPMODEL-based approach the free drainage lower boundary condition is replaced by a no flux condition, and sub-surface
20 runoff is represented as a lateral "baseflow", described below. An extra soil layer, with simplified representation of water fluxes, is added beneath the standard soil model as a computationally efficient way in which to track the water table when it is deeper than the standard 3 m soil column. JULES assumes an exponential decrease of K_s in this deeper layer with a decay constant f. The lateral sub-surface runoff, or baseflow (R_b),
25 is calculated as

$$R_b = T(\bar{z}_w) \exp(-\bar{\lambda}_i) \tag{55}$$

where $T(\bar{z}_w)$ is the vertical transmissivity from the bottom of the column to the $\bar{z}_w$, and $\bar{\lambda}_i$ is the gridbox-average topographic index. This transmissivity is found by summing the

Printer-friendly Version

Interactive Discussion

contributions from each layer and only considers unfrozen soil water. The transmissivity of each layer is used to partition the total baseflow between soil layers, to give the layer values R_{bn} required in Eq. (50). $\bar{z}_w$ is calculated by assuming that the column soil moisture is in equilibrium (Koster et al., 2000).

The "critical" value of the topographic index at which the water table reaches the surface is found as $\lambda_{ic} = \ln(R_{b\,max}/R_b)$, where $R_{b\,max}$ is the baseflow found from Eq. (55) with $\bar{z}_w = 0$. The fraction of the gridbox that is saturated (f_{sat}) can be found by integrating the pdf of the topographic index. However, this requires numerical integration if a two-parameter gamma distribution is used for the pdf as in Gedney and Cox (2003). Instead, during the initialisation an exponential distribution is fitted to the results of the gamma distribution, and subsequently f_{sat} is found using

$$f_{sat} = a_s \exp(-c_s f \lambda_{ic}) \tag{56}$$

where a_s and c_s are fitted parameters for each gridbox.

Saturation excess surface runoff (R_{se}) is then calculated as

$$R_{se} = f_{sat} W_0 \tag{57}$$

where W_0 is the rate at which water arrives at the soil surface from precipitation and snowmelt (Eq. 46).

The fraction of the gridbox that is considered to be wetland (i.e., stagnant water) for the purposes of methane emissions (f_{wet}) is defined as that part of the gridbox at which $\lambda_{ic} \leq \lambda_i \leq \lambda_{i\,max}$ where $\lambda_{i\,max}$ is a global parameter. At locations with larger values of λ_i (water higher above surface) the water is assumed to be flowing and not wetland. Following the procedure for f_{sat}, an exponential relationship is fitted so that f_{wet} can subsequently be calculated as $f_{wet} = a_{wt} \exp(-c_{wt} f \lambda_{ic})$ for parameters a_{wt} and c_{wt}. Gedney and Cox (2003) and Clark and Gedney (2008) showed that simulated runoff was improved by using a TOPMODEL type parameterisation, and that the global pattern of wetland is captured by this model (Gedney and Cox, 2003).

4.7.2 Probability distribution model (PDM)

An alternative to TOPMODEL is to calculate saturation excess runoff following the Probability Distributed Model (PDM, Moore, 1985). The distribution of soil storage capacity within a gridbox is modelled by a pdf, and the saturated fraction of the gridbox can be shown to be

$$f_{sat} = 1 - [1 - \theta/\theta_{max}]^{B/(B+1)} \tag{58}$$

where θ is the gridbox soil water content, θ_{max} is the storage at saturation and B is a shape parameter. R_{se} is then calculated using Eq. (57). In JULES, B is kept constant across the domain, as is the depth over which W and W_{max} are calculated (typically 1 m). The calculations of infiltration excess and sub-surface runoff are not altered if PDM is selected. Clark and Gedney (2008) showed that the use of PDM improved modelled runoff in mesoscale catchments.

5 Summary

The Joint UK Land Environment Simulator (JULES) is a new community land surface model, based upon the established Met Office Surface Exchange Scheme (MOSES). In addition to representing the exchange of fluxes of heat and moisture between the land surface and the atmosphere (as described here), the model also represents fluxes of carbon and some other gases such as ozone and methane (described in Clark et al., 2011). This enables JULES to be used for many applications including weather forecasting, earth system modelling and climate impacts.

The JULES model has been designed with a flexible and modular structure, which means that new elements of science can easily be introduced as new modules into the model. The scientific developments for each module are co-ordinated by an expert in the relevant area of science, ensuring that the model will remain a state of the art land surface model for the research community.

References

Beljaars, A. C. M. and Holtslag, A. A. M.: Flux parametrisation over land surfaces for atmospheric models, J. Appl. Meteorol., 30, 327–341, 1991. 601

Best, M. J.: Representing urban areas within operational numerical weather prediction models, Bound.-Lay. Meteorol., 114, 91–109, 2005. 606

Best, M. J., Beljaars, A., Polcher, J., and Viterbo, P.: A proposed structure for coupling tiled surfaces with the planetary boundary layer, J. Hydrometeorol., 5, 1271–1278, 2004. 601

Best, M. J., Cox, P. M., and Warrilow, D.: Determining the optimal soil temperature scheme for atmospheric modelling applications, Bound.-Lay. Meteorol., 114, 111–142, 2005. 619

Best, M. J., Grimmond, C. S. B., and Villani, M. G.: Evaluation of the urban tile in MOSES using surface energy balance observations, Bound.-Lay. Meteorol., 118, 503–525, 2006. 606

Beven, K. J. and Kirkby, M. J.: A physically based, variable contributing area model of basin hydrology, Hydrol. Sci. B, 24, 43–69, 1979. 599, 623

Blyth, E., Clark, D. B., Ellis, R., Huntingford, C., Los, S., Pryor, M., Best, M., and Sitch, S.: A comprehensive set of benchmark tests for a land surface model of simultaneous fluxes of water and carbon at both the global and seasonal scale, Geosci. Model Dev. Discuss., 3, 1829–1859, doi:10.5194/gmdd-3-1829-2010, 2010. 598

Brooks, R. H. and Corey, A. T.: Hydraulic properties of porous media, Colorado State University Fort Collins, Colorado, USA, Papers, 3, 1964. 620, 633, 634

Clapp, R. B. and Hornberger, G. M.: Empirical equations for some soil hydraulic properties, Water Resour. Res., 14, 601–604, 1978. 620

Clark, D. B. and Gedney, N.: Representing the effects of of subgrid variability of soil moisture on runoff generation in a land surface model, J. Geophys. Res., 113, D10111, doi:10.1029/2007JD008940, 2008. 624, 625, 626

Clark, D. B., Mercado, L. M., Sitch, S., Jones, C. D., Gedney, N., Best, M. J., Pryor, M., Rooney, G. G., Essery, R. L. H., Blyth, E., Boucher, O., Harding, R. J., and Cox, P. M.: The Joint UK Land Environment Simulator (JULES), Model description – Part 2: Carbon fluxes and

vegetation, Geosci. Model Dev. Discuss., 4, 641–688, doi:10.5194/gmdd-4-641-2011, 2011. 598, 603, 626

Collatz, G. J., Ball, J. T., Grivet, C., and Berry, J. A.: Physiological and environmental regulation of stomatal conductance, photosynthesis and transpiration: a model that includes a laminar boundary layer, Agr. Forest Meteorol., 54, 107–136, 1991. 602

Collatz, G. J., Ribas-Carbo, M., and Berry, J. A.: Coupled photosynthesis-stomatal conductance model for leaves of C_4 plants, Aust. J. Plant Physiol., 19, 519–538, 1992. 602

Cosby, B. J., Hornberger, G. M., Clapp, R. B., and Ginn, T. R.: A statistical exploration of the relationships of soil moisture characteristics to the physical properties of soils, Water Resour. Res., 20, 682–690, 1984. 620

Cox, P. M., Huntingford, C., and Harding, R. J.: A canopy conductance and photosynthesis model for use in a GCM land surface scheme, J. Hydrol., 213, 79–94, 1998. 602, 603

Cox, P. M., Betts, R. A., Bunton, C. B., Essery, R. L. H., Rowntree, P. R., and Smith, J.: The impact of new land surface physics on the GCM simulation of climate and climate sensitivity, Clim. Dynam., 15, 183–203, 1999. 597, 616, 619, 620, 621, 622, 634

Cox, P. M., Betts, R. A., Jones, C. D., Spall, S. A., and Totterdell, I. J.: Acceleration of global warming due to carbon-cycle feedbacks in a coupled climate model, Nature, 408, 184–187, 2000. 597

Cullen, M. J. P.: The unified forecast/climate model, Meteorol. Mag., 122, 81–94, 1993. 597

Deardorff, J. W.: Efficient prediction of ground surface temperature and moisture with inclusion of a layer of vegetation, J. Geophys. Res., 83, 1889–1903, 1978. 596

Dharssi, I., Vidale, P. L., Verhoef, A., Macpherson, B., Jones, C., and Best, M.: New soil physical properties implemented in the Unified Model at PS18, Met Office Technical Report 528, Met Office, Exeter, UK, 2009. 621, 622, 634

Dyer, A. J.: A review of flux-profile relationships, Bound.-Lay. Meteorol., 7, 363–372, 1974. 601

Essery, R. L. H., Best, M. J., Betts, R. A., Cox, P. M., and Taylor, C. M.: Explicit representation of subgrid heterogeneity in a GCM land surface scheme, J. Hydromet., 4, 530–543, 2003. 596, 597, 607, 609

Fisher, J. B., Sitch, S., Malhi, Y., Fisher, R. A., Huntingford, C., and Tan, S. Y.: Carbon cost of plant nitrogen acquisition: a mechanistic, globally applicable model of plant nitrogen uptake, retransocation, and fixation, Global Biogeochem. Cy., 24, GB1014, doi:10.1029/2009GB003621, 2010. 597

Gedney, N. and Cox, P. M.: The sensitivity of global climate model simulations to the

representation of soil moisture heterogeneity, J. Hydromet., 4, 1265–1275, 2003. 624, 625, 634

van Genuchten, M. T.: A closed-form equation for predicting the hydraulic conductivity of un-saturated soils., Soil Sci. Soc. Am. J., 44, 892–898, 1980. 620, 633, 634

5 Harman, I. N. and Belcher, S. E.: The surface energy balance and boundary layer over urban street canyons, Q. J. R. Meteorol. Soc., 132, 2749–2768, 2006. 606

Harman, I. N., Barlow, J., and Belcher, S. E.: Scalar fluxes from urban street canyons part II: model, Bound.-Lay. Meteorol., 113, 387–410, doi:10.1023/B:BOUN.0000045526.07270.a3, 2004. 607

10 Jacobs, C. M. J.: Direct impact of atmopsheric CO_2 enrichment on regional transpiration, Ph.D. thesis, Wageningen Agricultural University, Wageningen, 1994. 602

Jogireddy, V., Cox, P. M., Huntingford, C., Harding, R. J., and Mercado, L. M.: An improved description of canopy light interception for use in a GCM land-surface scheme: calibration and testing against carbon fluxes at a coniferous forest, Hadley Centre Technical Note 63,

15 Hadley Centre, Met Office, Exeter, UK, 2006. 603

Johansen, O.: Thermal conductivity of soils, Ph.d. thesis, University of Trondheim, Norway, 1975. 621

Kojima, K.: Densification of seasonal snow cover, in: Proc. International Conference on Low Temperature Science, Sapporo, Japan, 929–952, 14–19 August 1966, 1967. 612

20 Koster, R. D., Suarez, M. J., Ducharne, A., Stieglitz, M., and Kumar, P.: A catchment-based approach to modeling land surface processes in a general circulation model, J. Geophys. Res., 105, 24809–24822, 2000. 625

Leuning, R.: A critical appraisal of a combined stomatal-photosynthesis model for C_3 plants, Plant Cell Environ., 18, 357–364, 1995. 602

25 Lynch-Stieglitz, M.: The development and validation of a simple snow model for the GISS GCM, J. Climate, 7, 1842–1855, 1994. 612

Macdonald, R. W., Griffiths, R. F., and Hall, D.: An improved method for the estimation of surface roughness of obstacle arrays, Atmos. Environ., 32, 1857–1864, 1998. 606

Mercado, L. M., Huntingford, C., Gash, J. H. C., Cox, P. M., and Jogireddy, V.: Improving the

30 representation of radiative interception and photosynthesis for climate model applications, Tellus B, 59, 553–565, 2007. 603

Monin, A. S. and Obukhov, A. M.: Basic regularity in turbulent mixing in the surface layer of the atmosphere, Moscow, Ak. Nauk, Geof. Inst., 24, 163–187, 1954. 601

JULES energy and water

M. J. Best et al.

Monsi, M. and Saeki, T.: Ueber den Lichtfaktor in den Pflanzengesellschaften und seine Bedeutung fuer die Stoffproduktion, Jpn. J. Bot., 14, 22–52, 1953. 603

Moore, R. J.: The probability-distributed principle and runoff production at point and basin scales, Hydrol. Sci. J., 30, 273–297, 1985. 599, 626, 634

Pitman, A. J., Liang, Z. L., Cogley, J. G., and Henderson-Sellers, A.: Description of bare essentials of surface transfer for the Bureau of Meteorological Research Centre AGCM, Bureau of Meteorology, Melbourne, Australia, BMRC Research Report No. 32, 1991. 612

Porson, A., Harman, I. N., Bohnenstengel, S. I., and Belcher, S. E.: How many facets are needed to represent the surface energy balance of an urban area?, Bound.-Lay. Meteorol., 132, 107–128, 2009. 606

Porson, A., Clark, P. A., Harman, I. N., Best, M. J., and Belcher, S. E.: Implementation of a new urban energy budget scheme in the MetUM. Part I. Description and idealized simulations, Q. J. R. Meteorol. Soc., 136, 1514–1529, 2010a. 606, 607, 634

Porson, A., Clark, P. A., Harman, I. N., Best, M. J., and Belcher, S. E.: Implementation of a new urban energy budget scheme in the MetUM. Part II. Validation against observations and model intercomparison, Q. J. R. Meteorol. Soc., 136, 1530–1542, 2010b. 606, 634

Schlosser, C. A., Slater, A. G., Pitman, A. J., Vinnikov, K. Y., Henderson-Sellers, A., Speranskaya, N. A., and Mitchell, K.: Simulations of a boreal grassland hydrology at Valdai, Russia: PILPS phase 2(d), Mon. Weather Rev., 128, 301–321, 2000. 623

Sellers, P. J.: Canopy reflectance, photosynthesis, and transpiration III. A reanalysis using improved leaf models and a new canopy integration scheme, Int. J. Remote Sens., 6, 1335–1372, 1985. 608

Sivapalan, M., Wood, E. F., and Beven, K. J.: On hydrologic similarity. 2. A scaled model of storm runoff production. 3. A dimensionless flood frequency model using a generalised geomorphologic unit hydrograph and partial area runoff generation, Water Resour. Res., 26, 43–58, 1987. 624

Sokolov, A. P., Kicklighter, D. W., Melillo, J. M., Felzer, B. S., Schlosser, C. A., and Cronin, T. W.: Consequences of considering carbon-nitrogen interactions on the feedbacks between climate and the terrestrial carbon cycle, J. Climate, 21, 3776–3796, doi:10.1175/2008JCLI2038.1, 2008. 597

Thornton, P. E., Lamarque, J. F., Rosenbloom, N. A. and Mahowald, N. M.: Influence of carbon-nitrogen cycle coupling on land model response to CO_2 fertilization and climate variability, Global Biogeochem. Cy., 21, GB4018, doi:10.1029/2006GB002868, 2007. 597

Thornton, P. E., Doney, S. C., Lindsay, K., Moore, J. K., Mahowald, N., Randerson, J. T., Fung, I., Lamarque, J.-F., Feddema, J. J., and Lee, Y.-H.: Carbon-nitrogen interactions regulate climate-carbon cycle feedbacks: results from an atmosphere-ocean general circulation model, Biogeosciences, 6, 2099–2120, doi:10.5194/bg-6-2099-2009, 2009. 597

5 Wiscombe, W. J. and Warren, S. G.: A model for the spectral albedo of snow. 1. Pure snow, J. Atmos. Sci., 37, 2712–2733, 1980. 615

Zaehle, S., Friend, A. D., Friedlingstein, P., Dentener, F., Peylin, P., and Schulz, M.: Carbon and nitrogen cycle dynamics in the O-CN land surface model: 2. Role of the nitrogen cycle in the historical terrestrial carbon balance, Global Biogeochem. Cy., 24, GB1006,
10 doi:10.1029/2009GB003522, 2010. 597

Back   Close

Full Screen / Esc

Printer-friendly Version

Interactive Discussion

Table 1. Meteorological forcing data required to drive the JULES model.

Data	Units
Downward component of shortwave radiation at the surface	$W\,m^{-2}$
Downward component of longwave radiation at the surface	$W\,m^{-2}$
Rainfall	$kg\,m^{-2}\,s^{-1}$
Snowfall	$kg\,m^{-2}\,s^{-1}$
U component of wind	$m\,s^{-1}$
V component of wind	$m\,s^{-1}$
Atmospheric temperature	K
Atmospheric specific humidity	$kg\,kg^{-1}$
Surface pressure	Pa

Table 2. Soil ancillary data required by the JULES model for initialisation.

Data	Units
Bare soil albedo	
Dry soil thermal conductivity	$\mathrm{W\,m^{-1}\,K^{-1}}$
Dry soil thermal capacity	$\mathrm{J\,K^{-1}\,m^{-3}}$
Volumetric saturation point for soil	$\mathrm{m^3\,m^{-3}}$ of soil
Critical volumetric soil moisture content	$\mathrm{m^3\,m^{-3}}$ of soil
Volumetric wilting point for soil	$\mathrm{m^3\,m^{-3}}$ of soil
Soil saturated hydraulic conductivity of soil	$\mathrm{kg\,m^{-2}\,s^{-1}}$
Saturated soil water pressure (Brooks and Corey, 1964, only)	m
Clapp-Hornberger exponent (Brooks and Corey, 1964, only)	
$1/\alpha$ (van Genuchten, 1980, only)	
$1/(n-1)$ (van Genuchten, 1980, only)	

Table 3. Description of the various physics options within the JULES model.

Physics	Option
Surface exchange	No thermal inertia and conductive coupling
	No thermal inertia and radiative coupling
	Thermal inertia and radiative coupling
	Thermal inertia, radiative coupling and snow under vegetation canopy
Canopy radiation and scaling	Big leaf
	Multiple canopy layers
	2 layer approximation to multiple canopy layers
	Multiple canopy layers with variable leaf nitrogen
Albedo	Bulk albedos
	Spectral albedos and snow ageing
Urban model	1 tile (bulk)
	2 tiles (roofs and canyons)
	MORUSES (Porson et al., 2010a,b)
Snow	Zero layer model
	Multi-layer model
Soil moisture super-saturation	Restricted drainage into layer
	Infiltration into lower layer
Soil thermodynamics	Cox et al. (1999)
	Dharssi et al. (2009)
Soil hydraulics	Brooks and Corey (1964)
	van Genuchten (1980)
Large scale hydrology	TOPMODEL (Gedney and Cox, 2003)
	PDM (Moore, 1985)

Table 4. Definitions of symbols used for the surface energy balance, Eqs. (1)–(4).

Symbol	Definition
C	Heat capacity associated with the surface material
T_*	Surface temperature
$Sw_\downarrow$	Downward component of the solar radiation
$Lw_\downarrow$	Downward component of the longwave radiation
ϵ	Surface emissivity
σ	Stefan Boltzmann constant
α	Surface albedo
H	Turbulent heat flux
E	Turbulent latent heat flux
G	Surface soil heat flux
L_c	Latent heat of condensation of water at $0\,^\circ$C
ρ	Density of air
c_p	Specific heat capacity of air
r_a	Aerodynamic resistance
T_1	Reference level atmospheric temperature
r_s	Stomatal or surface moisture resistance
$Q_{sat}(T_*)$	Saturated specific humidity at the surface temperature
Q_1	Specific humidity at the reference atmospheric level
v	Fraction of vegetation
ϵ_s	Emissivity of the underlying soil surface
T_{s1}	Temperature of the first soil level
$r_{a_{can}}$	Aerodynamic resistance between the surface canopy of vegetation and the underlying soil
A_s	Thermal conductivity of the soil

Table 5. Default parameter values requied by JULES for the standard vegetation surfaces.

Parameter	Broadleaf trees	Needleleaf trees	C_3 grasses	C_4 grasses	Shrubs
Snow-covered albedo for large LAI	0.15	0.15	0.60	0.60	0.40
Snow-covered albedo for zero LAI	0.30	0.30	0.80	0.80	0.80
Snow-free albedo for large LAI	0.10	0.10	0.20	0.20	0.20
Rate of change of vegetation roughness length with height	0.05	0.05	0.10	0.10	0.10
Minimum canopy capacity ($kg\,m^{-2}$)	0.50	0.50	0.50	0.50	0.50
Rate of change of canopy capacity with LAI	0.05	0.05	0.05	0.05	0.05
Infiltration enhancement factor	4.00	4.00	2.00	2.00	2.00
Light extinction coefficient	0.50	0.50	0.50	0.50	0.50
Rootdepth (m)	3.00	1.00	0.50	0.50	0.50

Table 6. Default parameter values requied by JULES for standard non-vegetation surfaces.

Parameter	Urban	Water	Soil	Ice
Snow-covered albedo	0.40	0.80	0.80	0.80
Snow-free albedo	0.18	0.06	-1.00^{a}	0.75
Canopy capacity ($kg\,m^{-2}$)	0.50	0.00	0.00	0.00
Surface conductance ($m\,s^{-1}$)	0.00	0.00	1×10^{-2}	1×10^{6}
Infiltration enhancement factor	0.10	0.00	0.50	0.00
Roughness length (m)	1.00	3×10^{-4}	3×10^{-4}	1×10^{-4}
Canopy heat capacity ($J\,K^{-1}\,m^{-2}$)	0.28×10^{6}	0.00	0.00	0.00
Fractional "canopy" coverage	1.00	0.00	0.00	0.00

[a] The snow-free albedo for soil is initialised to −1 to allow it to be set through an ancillary field instead.
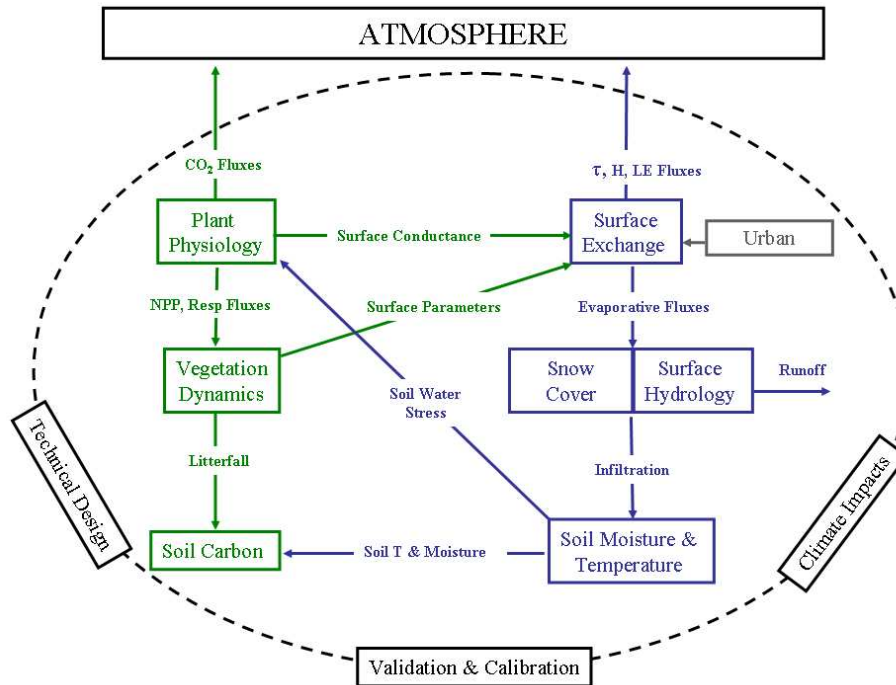
Fig. 1. Modular structure of the JULES model. The boxes show each of the physics modules whilst the lines between the boxes show the physical processes that connect these modules. The surrounding three boxes show the cross-cutting themes.

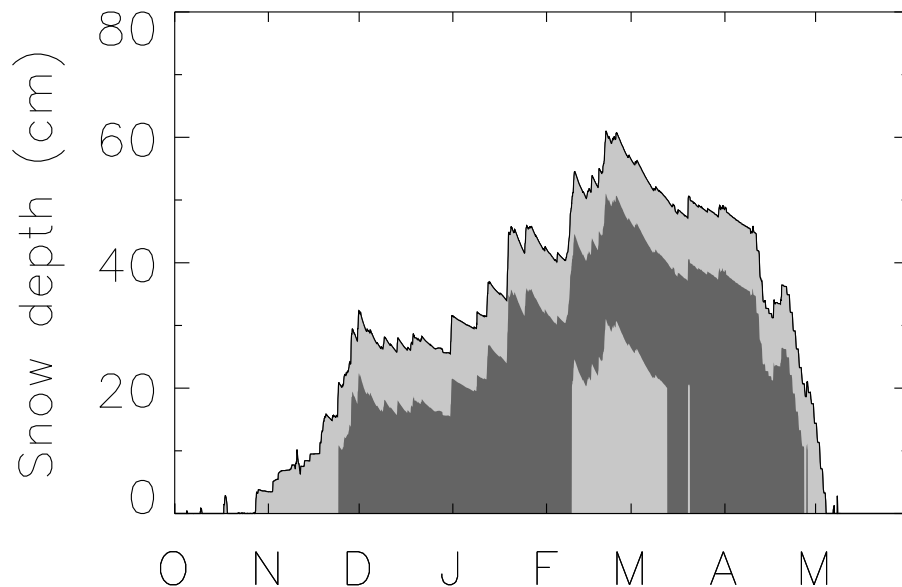Full Screen / Esc

Printer-friendly Version

Interactive Discussion

Fig. 2. Simulation of seasonal snow depth with JULES for multi-level snow scheme, showing the division into a varying number of layer depths. The full shaded area shows the total snow depth, whilst the different shadings represent the depths of the various snow layers.
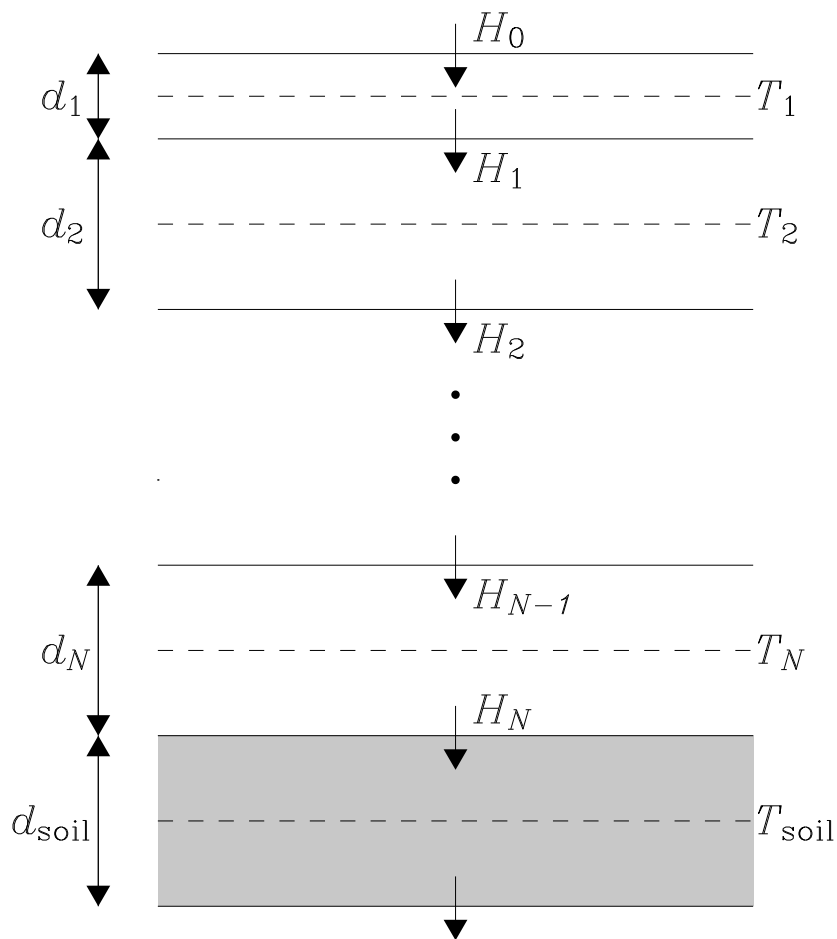
Fig. 3. Structure of the numerical discretisation over the layers for the temperatures and heat fluxes within the multi-level snow scheme in JULES.